Well-dispersed clay in photopolymerized poly(ionic liquid) matrix

Salminen, Linda

2022-12-01

Salminen , L , Karjalainen , E , Aseyev , V & Tenhu , H 2022 , ' Well-dispersed clay in photopolymerized poly(ionic liquid) matrix ' , Materials Chemistry and Physics , vol. 292 , 126805 . https://doi.org/10.1016/j.matchemphys.2022.126805

http://hdl.handle.net/10138/350381
https://doi.org/10.1016/j.matchemphys.2022.126805

Materials Chemistry and Physics 292 (2022) 126805

Contents lists available at ScienceDirect

Materials Chemistry and Physics

journal homepage: www.elsevier.com/locate/matchemphys

Well-dispersed clay in photopolymerized poly(ionic liquid) matrix

Linda Salminen [a], Erno Karjalainen [b,*], Vladimir Aseyev [a,**], Heikki Tenhu [a]

[a] Department of Chemistry, University of Helsinki, P.O. Box 55 (A.I. Virtasen aukio 1), FIN-00014 HY, Helsinki, Finland
[b] VTT Technical Research Centre of Finland Ltd., P.O. Box 1000, FI-02044 VTT, Espoo, Finland

HIGHLIGHTS

- A facile methodology for polymer composite synthesis is introduced.
- Polymerizable ionic liquid is used as filler dispersant and matrix constituent.
- Marked improvements in mechanical properties are achieved by addition of filler.

GRAPHICAL ABSTRACT

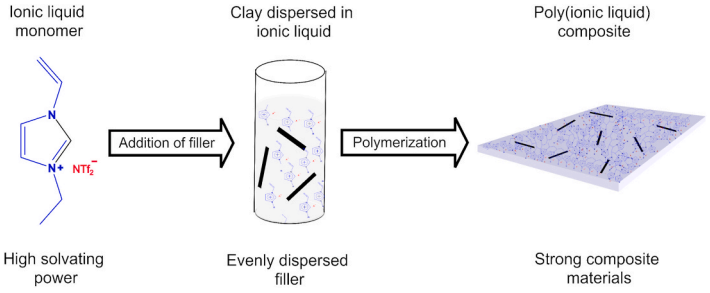

ARTICLE INFO

Keywords:
A. Particle-reinforcement
B. Mechanical properties
B. Thermal properties
D. Failure

ABSTRACT

This contribution presents a methodology for combining the solvating power of ionic liquids with polymer composite synthesis. A polymerizable ionic liquid was used as solvent to disperse clay, after which the mixture was polymerized into a solid polymer-clay composite. Polymer-clay composites were prepared with filler loadings up to 10 wt%. The addition of clay as filler enhanced mechanical properties; tensile strength and stiffness of the materials exhibited appreciable improvements. The glass transition temperature of the materials shifted to slightly higher temperatures due to the hindered segmental motions of the polymer chains. The improvements were the highest at approximately 5 wt% filler content. When the filler content was increased further, excessive aggregate formation impaired the material properties.

1. Introduction

Layered silicates are popular filler materials in composites due to the improvements in mechanical [1–3], flame-resistant [4,5], and barrier [6] properties they offer compared to plain polymers. Especially montmorillonite clay has been utilised in polymer-clay composites for a long time [7]. The high aspect ratio of clay particles makes clay fitting for reinforcement [7]. However, clay nanolayers tend to stack and form aggregates [7]. Since clay is incompatible with commonly used polymers, dispersion of the aggregates is difficult. The incompatibility can be mitigated by modifying the clay. In particular, by exchanging the clay's inorganic interlayer cations with organic ones, which turn the surface more organophilic and thus more compatible with polymers [2,8,9]. Still, dispersion of clay can prove to be challenging even with such modifications.

Since the properties of polymer composites are generally sensitive to

* Corresponding author.
** Corresponding author.
E-mail addresses: erno.karjalainen@alumni.helsinki.fi (E. Karjalainen), vladimir.aseyev@helsinki.fi (V. Aseyev).

https://doi.org/10.1016/j.matchemphys.2022.126805
Received 30 June 2022; Received in revised form 17 September 2022; Accepted 19 September 2022
Available online 28 September 2022

the quality of filler dispersion [10–16], ensuring even filler dispersion is imperative in polymer composite synthesis. In this work, fillers are dispersed with the aid of ionic liquids since ionic liquids are known for their ability to dissolve or disperse various materials [17–22].

Polymerization of ionic liquids provides poly(ionic liquids), that are also known as polymerized ionic liquids (PILs) [23]. PILs retain the extensive tunability of ionic liquids, while their polymeric nature offers excellent processability [23,24]. Physical properties, such as glass transition temperature (T_g) and water solubility, of ILs [25–27] and PILs [28–33] can be adjusted by the choice of small molecular anions. This makes PILs interesting for various applications. Nonetheless, only a few examples of free-standing PIL films have been reported [34–40]. Reports on PIL composites that use ionic liquids as dispersants are rare; the earliest ones use carbon nanotubes as a filler material [41–44]. Later on, other filler materials, i.e. cellulose, have been used in a similar manner [14,45–52].

The objective of this research is – by utilising the solvating power of ionic liquids – to develop a systematic methodology for the synthesis of PIL composites. The methodology is to disperse clay in a polymerizable ionic liquid at room temperature, which is then polymerized into a solid composite. Dispersing a filler in a monomeric ionic liquid, as opposed to a PIL, offers more even filler dispersion, and eliminates the need of a solvent. Furthermore, with this methodology the polymerization and composite fabrication are realised in one, straightforward step.

Polymer-clay composites were prepared with various filler loadings. The composites' mechanical and thermal properties were determined with stress-strain measurements, dynamic mechanical analysis, differential scanning calorimetry, and thermogravimetric analysis. Furthermore, the fracture surface morphologies were characterised by means of scanning electron microscopy (SEM). The properties of polymer composite materials are presented focusing on changes in material properties with increasing filler content.

2. Experimental section

2.1. Materials

1-Vinylimidazole (Aldrich, >99%) was passed through basic aluminium oxide and filtered. 2,2′-Azobis(2-methylpropionitrile) (AIBN) (Aldrich, 98%), was recrystallized from methanol. Bromoethane (Aldrich, 98%), 1,8-dibromooctane (Aldrich, 98%), diphenyl(2,4,6-trimethylbenzoyl)phosphine oxide (Aldrich, 97%), bis(trifluoromethane)sulfonimide lithium salt ($LiNTf_2$) (Aldrich, >99%), and montmorillonite clay (Aldrich, K 10) were used as received.

2.2. Syntheses

2.2.1. 1-vinyl-3-ethyl imidazolium bromide (VEImBr)

1-Vinylimidazole (15.0023 g, 159.4 mmol) and excess bromoethane (52.4956 g, 481.7 mmol) were mixed and purged with nitrogen for 15 min. The mixture was refluxed at 40 °C for 17 h. The solidified reaction mixture was precipitated twice from chloroform into ethyl acetate. The product was dried under vacuum. The yield was 88.0%. Purity of the product was verified with ^{1}H NMR. The IR spectrum of the product is available in Supplementary Information (SI) (Fig. S1A).

2.2.2. 1-vinyl-3-ethyl imidazolium bis(trifluoromethane)sulfonimide (M1)

$LiNTf_2$ (23.3207 g, 81.2 mmol) was dissolved in 20 mL of water and VEImBr (15.0353 g, 74.0 mmol) was dissolved in 20 mL of dichloromethane. $LiNTf_2$ solution was added dropwise to vigorously stirred VEImBr solution. The reaction was stirred at room temperature for 16 h, after which the phases were separated. The aqueous phase was extracted with dichloromethane (2*30 mL) and the combined organic phases were washed with water (3*100 mL). The organic phase was dried over 3 Å molecular sieves. The solvent was then evaporated, and the remaining ionic liquid was dried under vacuum for 5 h. Purity of the product was verified with ^{1}H NMR (92.2% yield). The IR spectrum of the monomer is shown in Fig. S1A.

2.2.3. 1,1′-octane-1,8-diylbis(3-vinyl imidazolium) di[bis (trifluoromethane)sulfonimide] (CL)

1-Vinylimidazole (17.3018 g, 183.9 mmol) and 1,8-dibromooctane (5.0071 g, 18.4 mmol) were mixed and purged with nitrogen for 40 min. The mixture was let to react in 40 °C for 18 h. The product was precipitated into ethyl acetate and the precipitate was dissolved in water. The aqueous solution was washed three times with dichloromethane (3*100 mL). The washed aqueous phase was added into vigorously stirred aqueous $LiNTf_2$ (12.6833 g, 44.2 mmol $LiNTf_2$ in 200 mL of water). The mixture was filtered, and the precipitate dissolved in dichloromethane. The solution was washed with water (3*100 mL) and dried over 3 Å molecular sieves. Dichloromethane was evaporated and the resulting solid was dried under vacuum. Purity of the product was ascertained with ^{1}H NMR (80.6% yield). The IR spectrum of the product is given in Fig. S1A.

2.2.4. Poly(1-vinyl-3-ethyl imidazolium bromide) (PVEImBr)

VEImBr (22.7281 g, 111.9 mmol) and AIBN (0.1832 g, 1.1 mmol) were dissolved in 70 mL of methanol and purged with nitrogen for 1 h. The reaction was started by heating the mixture to 60 °C, and the reaction was terminated after 24 h. The polymer was separated by dialysing against water for 5 days, switching the water 5 times during the process. The polymer was isolated by freeze-drying (Yield 12.0937 g). The IR spectrum of the polymer is shown in Fig. S1B.

2.2.5. Poly(1-vinyl-3-ethyl imidazolium bis(trifluoromethane)sulfonimide) (Poly(M1))

PVEImBr (0.5054 g, 2.5 mmol repeating units) was dissolved in 15 mL of water and combined with a 15 mL water solution, which contained $LiNTf_2$ (0.7870 g, 2.7 mmol). After mixing at ambient temperature for 16 h, the precipitate was filtered out and washed with water. The polymer was dried and the yield was 0.8587 g (85.55%). The IR spectrum of the polymer is shown in Fig. S1B.

2.2.6. Organoclay (OMMT)

Montmorillonite clay (MMT), which is cation-exchanged with 1-vinyl-3-ethyl imidazolium bromide (VEImBr). Montmorillonite clay (5.0064 g) was dispersed in 60 mL of water. Then VEImBr (2.0438 g) that had been dissolved in 10 mL of water was added to the clay dispersion. The mixture was stirred for 23 h at room temperature. The organoclay was washed with water until $AgNO_3$-test no longer indicated presence of halide anions in washing water. The organically modified clay was dried under vacuum. (4.6250 g yield).

2.3. General procedure for film preparation (exemplified with a film with 2 mol% crosslinker and 5 wt% OMMT)

The crosslinker (0.2622 g, 0.3 mmol), OMMT (0.3184 g), and M1 (6.0079 g, 14.9 mmol) were mixed in a vial at room temperature until apparent homogeneity was achieved. The mixture was then sonicated for 15 min in an ice bath to improve the dispersion. The sonication was made in 0.5s cycles with 100% amplitude using a Hielscher UP400S ultrasonic processor. Then, a photoinitiator diphenyl(2,4,6-trimethylbenzoyl)phosphine oxide (0.1056 g, 0.3 mmol) was added to the mixture. The mixture was transferred to a mould and photopolymerized under UV light (1.5 h) at wavelength of 365 nm using a setup with four 9 W tubes. The ready composite was removed from the mould and rinsed with methanol in order to remove the remains of unreacted monomer. The washed composite film was dried and the purity of the film was ascertained with FTIR spectroscopy by checking the absence of alkene related bands, i.e. C=C stretching around 1650 cm^{-1} and C–H bending around 950 cm^{-1} from the IR spectra. As an example, the IR spectra of the IL monomer (M1) and a crosslinked film of

polymerized M1 are given in Fig. S2 in Supplementary Information (SI).

The rest of the films were prepared in a similar manner. The films of crosslinked poly(M1) were prepared in the same manner with the exception that no clay was added into the mixture.

2.4. Instrumentation

2.4.1. Thermogravimetric measurements

Thermogravimetric measurements were made with Netzsch STA 449 F3. The samples were heated 25–800 °C 10 °C/min under nitrogen atmosphere.

2.4.2. Oscillatory modulus measurements

The viscoelastic properties of the films were determined by measuring their storage and loss moduli as a function of temperature. The measurements were conducted with a TA Instruments DMAQ800 –instrument. The measurements were performed using a 0.1% strain amplitude with 1 Hz frequency. The samples were heated from 25 to 250 °C, 5 °C/min.

2.4.3. Differential scanning calorimetry

Calorimetric measurements were carried out on a TA Instruments DSC Q2000 calorimeter. The samples were heated from 25 to 250 °C, 10 °C/min.

2.4.4. Tensile testing

TA Instruments Discovery HR-2 hybrid rheometer was used to measure the composites' stress-strain curves. The elongation speed was 10 μm/s and the composites were stretched until breakage. The measurements were made at 25 °C or 140 °C and the samples were stabilised at the target temperature for 10 min before starting the measurements. In general, three measurements were made and the results were averaged.

2.4.5. Scanning electron microscopy (SEM)

The composites' fracture surfaces, i.e. fractures that occurred during stress-strain measurements, were examined using Hitachi S-4800 FESEM with an acceleration voltage of 3 kV. The samples were coated with a thin layer of Au–Pd prior to measurements to avoid charging.

2.4.6. Energy dispersive X-ray spectroscopy (EDX)

EDX elemental mapping was made with Hitachi S-4800 equipped with Oxford INCA 350 EDX microanalysis system.

3. Results and discussion

The studied composites are glassy materials that are prepared by photopolymerizing a mixture of ionic liquid as a monomer M1, crosslinker (CL), and organically modified montmorillonite clay, i.e. organoclay (OMMT). The main constituent of the composites, M1, is an imidazolium salt that is in a liquid state at room temperature. M1 has been used before in preparation of polymer films, but the materials proved to be too brittle for evaluation of mechanical properties [41]. In this work, the materials were chemically crosslinked to improve their durability. The structures of M1 and CL are depicted in Fig. 1 and their NMR spectra are given in Supplementary Information (Fig. S3).

The filler material, montmorillonite clay, is a layered aluminosilicate, which is formed of stacked silica- and aluminium sheets [53]. The clay platelets are separated by interlayer galleries that are typically occupied by Na^+ and K^+ ions [54,55]. The hydrophilic, hydrated cations within the galleries can be exchanged with organic cations, thus converting the normally hydrophilic surface to an organophilic surface [56–59]. In this work, montmorillonite clay was modified with the same cation that is present in the matrix-forming PIL to improve filler dispersion.

Composites were prepared with various filler loadings up to 10 wt%,

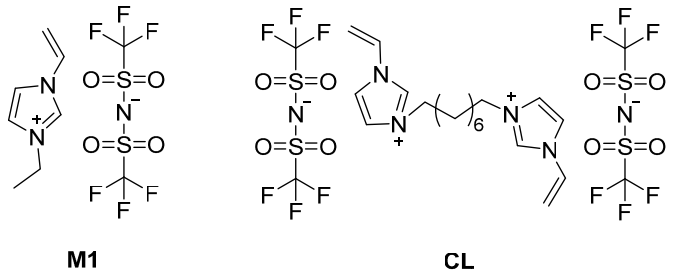

Fig. 1. Structures of the IL monomer (M1) and crosslinker (CL).

and the effect of filler on the material properties was studied. The next section presents the thermal properties of the prepared composites, and the following one their mechanical properties.

3.1. Thermal properties of PIL-OMMT composites

The thermal stability and thermal phase behaviour were studied with thermogravimetric analysis (TGA), differential scanning calorimetry (DSC), and dynamic mechanical analysis (DMA).

The success of cation intercalation was verified with IR spectroscopy and TGA. Fig. S4 in SI shows the IR spectra of unmodified montmorillonite clay and cation-exchanged organoclay. Compared to unmodified montmorillonite clay, the modified clay exhibits a small peak around 1550 cm^{-1}, which was ascribed to C═C stretching of the organic cation. The most prominent peak in the IR spectra around 1000 cm^{-1} arises from Si–O stretching and likely covers some other cation-related peaks. Therefore, the extent of intercalation was also studied with TGA. Fig. S5 in SI shows the TGA curves of montmorillonite clay and OMMT. The extent of intercalation was calculated with equation (1), where the organic composition was calculated from the TGA weight loss from 150 °C to 800 °C and bare MMT is the weight retention of unmodified montmorillonite clay [60]. TGA showed that the organic content of OMMT was 3.1 wt%.

$$Surfactant\ in\ OMMT(\%) = \frac{Organic\ composition}{Bare\ MMT} * 100\% \quad (1)$$

TGA measurements were performed to assess the thermal stability of the composites, and to determine a suitable temperature range for DMA and DSC measurements. That is, TGA measurements were used to make sure that DMA and DSC measurements were conducted well below the materials' decomposition temperature. The TGA curves are given in Fig. S6 in SI. The degradation onset temperature was defined as the temperature where, starting from 150 °C, 2% of the material had degraded. The obtained degradation temperatures and char residues have been listed in Table 1. As is commonly observed in polymer-clay composites, the composites exhibited increased thermal stability as

Table 1
The TGA results.

Organoclay (wt%)	Onset of degradation with 1 mol% CL (C)[a]	Onset of degradation with 2 mol% CL (C)[a]	Char residue with 1 mol % CL (wt %)	Char residue with 2 mol % CL (wt %)
0	357	354	7.2	6.6
1	357	359	8.3	8.5
5	358	359	13.5	13.4
7	359	356	14.6	14.9
10	354	357	16.8	17.2

[a] Defined as the temperature where, starting from 150 °C, 2% of the material has degraded.

filler was added [61]. However, the increase in degradation temperature is subtle. The lagging of the degradation point was ascribed to the ability of clay platelets to act as a barrier that hinders the diffusion of volatile degradation products from the composite. The composites were the most stable with 5–7 wt% organoclay, after which the degradation onset decreased. This arises from aggregation of the clay. Aggregated filler is not able to form an even barrier and thus cannot impart significant improvements in the thermal properties of the composite. Table 1 also shows that the char residue increases with increasing filler loading.

In order to verify the presence of clay aggregates, the composites' fracture surface morphology was characterised with scanning electron microscopy (SEM). Images of fracture surfaces of composites with 2% CL and various filler loadings are given below in Fig. 2. The SEM images of Fig. 2 are also available in larger size in SI (Fig. S7) for clearer viewing of the scale bars. Fig. 2 confirms the presence of clay aggregates. Since clay aggregates are present on the surface, it is reasonable to assume that the materials' fracturing involves breakage of clay aggregates.

A film with 1 wt% OMMT exhibits crack deflection, which is seen in the form of step defects. In the presence of rigid, inorganic particles, a propagating crack moves around the particles, thus resulting in an increased crack length [62]. The diverted crack exhibits a tail-like feature behind the particle.

The composites with 5 wt% and 7 wt% OMMT feature similar morphologies. Both composites exhibit clay agglomeration with clay tactoids visible at high magnifications (see Fig. 2F and I). However, lack of voids at the particle-matrix interface attests to well-bonded aggregates. The fracture surface morphology is a result of crack deflection and bifurcation, and separation between clay platelets.

The fracture surface morphology of 10 wt% OMMT composite features a variation of smooth and highly aggregated regions. Due to the large aggregate size, the separation between clay platelets is the dominant failure method.

A complementary study on filler dispersion was done by means of EDX. As an example, the elemental maps of a composite with 5 wt% OMMT are given in Fig. 3 below. The EDX maps for other filler loadings are given in Fig. S8 in SI. As evidenced by Fig. 3, Si and Al from montmorillonite clay were observed on the fracture surface of the composite. Si and Al appear in the form of microscale clusters that are dispersed

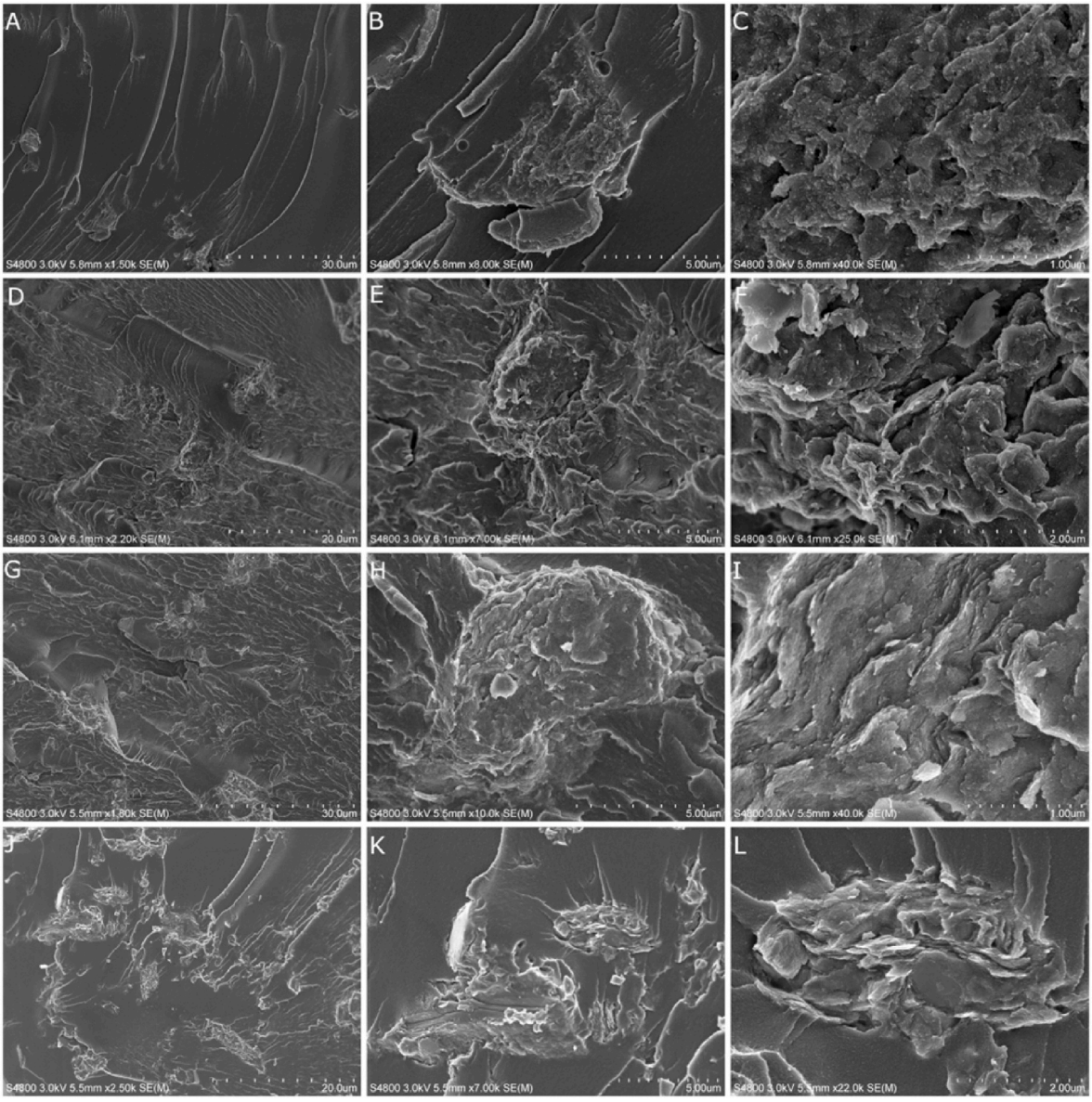

Fig. 2. SEM images of tensile fracture surfaces of composites with 1 wt% OMMT (A–C), 5 wt% OMMT (D–F), 7 wt% OMMT (G–I), and 10 wt% OMMT (J–L) with the magnification increasing from left to right.

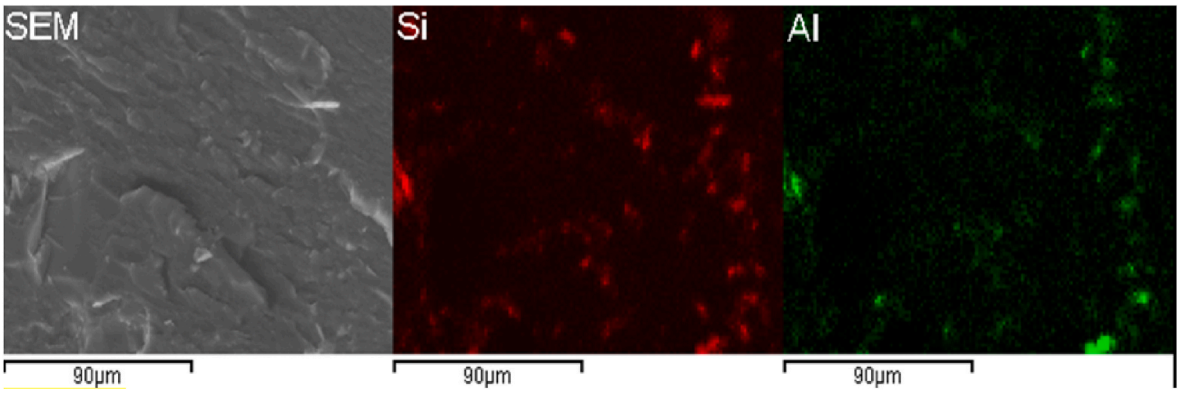

Fig. 3. SEM image and corresponding EDX maps on the fracture surface of a composite that contains 5 wt% OMMT.

throughout the material. Based on the Si signals, the largest aggregates are roughly 20 μm in diameter. However, the general aggregate size appears to be around 5–10 μm. The aggregate sizes are in line with the estimations made from the SEM images.

Fig. S8, which shows the EDX maps of composites with 1 wt%, 7 wt %, and 10 wt%, exhibits increasing aggregate number with increasing filler loading. With the lowest filler loading, 1 wt%, the general aggregate diameter is roughly estimated to be around 5 μm. Likewise, the more highly filled composites exhibit mainly 5–10 μm aggregates that are accompanied by occasional larger aggregates.

Dynamic mechanical analysis (DMA) was conducted to investigate the thermomechanical behaviour of the composites. The obtained tan δ curves for the composites with 1% crosslinker have been depicted in Fig. 4A and the curves for those with 2% crosslinker in Fig. 4B. All curves – for both filled and unfilled materials – are similar in shape. Each tan δ curve shows two peaks; first one around 90 °C, and the second one around 120 °C. The secondary transition has been encountered before with polymeric M1 [63]. The appearance of the shoulder can be rationalized to arise from ion pair motions and rotational motion of bis(trifluoromethane)sulfonimide anions [31,63–65]. This rationalization is supported by the fact that the shoulder is the most prominent in the absence of clay. The shoulder also appears to be more prominent with higher crosslinker content. With 1% crosslinker, the shoulder is subtle and does not have a distinguishable peak. In contrast, most composites with 2% crosslinker had shoulders with discernible peaks. Therefore, also the crosslinker may contribute to the secondary transition.

In summary, the appearance of two peaks in the tan δ curves was ascribed to the crosslinker or to the motion of ions and ion pairs, or a combination of both.

Fig. 4 also shows that the magnitude of the relaxation, the maximum height of tan δ, decreases with increasing filler content. The peak intensity also appears to decrease with increasing crosslinker-concentration. The magnitude of the relaxation process is lowered by both chemical crosslinks and the bonds between the filler and the matrix. The decrease in peak intensity indicates that the composite contains less mobile units at T_g with added crosslinker and filler. These changes in the dynamic mechanical behaviour can be ascribed to particle-particle slipping and friction, as well as particle-polymer motion at the interface [66].

The thermomechanical properties of composite materials are highly dependent on the filler material's extent of wetting [67]. Clay-additions have been shown to both increase and decrease the glass transition temperature (T_g) depending on the filler's compatibility with the matrix. When the particle surface is compatible with the matrix, T_g increases since the filler hinders the segmental movements of the polymer chains [68,69]. In contrast, if the filler particles are repulsive or dewetting, T_g decreases [70]. The glass transition temperatures of the composites are presented in Fig. 5 in dependence of the filler content. T_g is defined as the peak of tan δ curve. T_g is seen to increase with added filler up to 7 wt %, after which it decreases. The initial increase in T_g arises from filler-matrix adhesions that hinder chain mobility. However, as is seen in Fig. 2, the composites with high filler loadings contain many agglomerated filler particles. The agglomerated particles can slide by each other, which results in a lowered T_g compared to composites with less agglomerated clay [66]. However, even in this case the presence of clay increases the T_g.

The thermal transitions of the composites were also characterised by means of differential scanning calorimetry (DSC) and the T_gs are plotted in Fig. 5. The DSC traces of composites with varying filler loadings are given in SI (Fig. S9). Similarly, to what was observed with the DMA measurements, the T_g increases steadily up until 7 wt% filler content, after which it starts to decrease.

The T_gs determined with DMA and DSC differ greatly. The main reason for the difference is ascribed to the chosen definition of T_g in

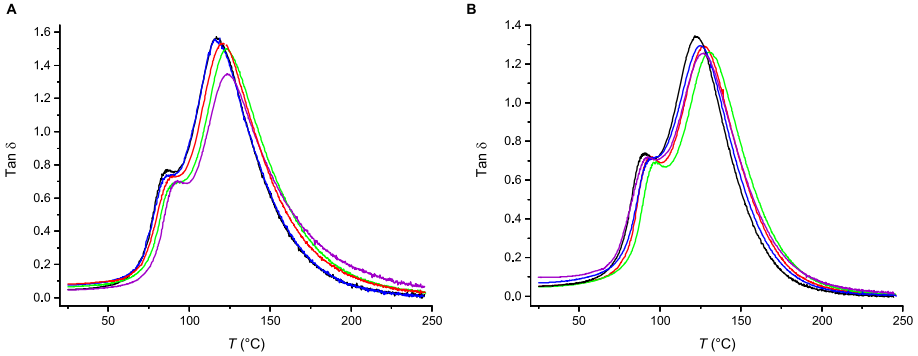

Fig. 4. Tan δ curves of composites with A) 1% and B) 2% crosslinker. The composites are filled with 0 wt% (black), 1 wt% (blue), 5 wt% (red), 7 wt% (green), or 10 wt% (purple) OMMT. (For interpretation of the references to colour in this figure legend, the reader is referred to the Web version of this article.)

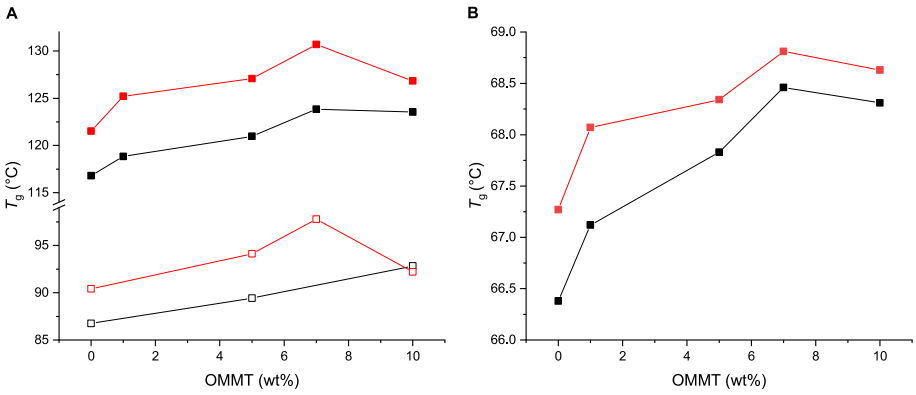

Fig. 5. Glass transition temperatures of composites with 1% (black) and 2% (red) crosslinker in dependence of OMMT content. A) T_gs obtained from DMA. The secondary transitions are given as open symbols and the main transition as filled symbols. B) T_gs obtained from DSC. (For interpretation of the references to colour in this figure legend, the reader is referred to the Web version of this article.)

DMA measurements. The peak of loss modulus and the drop in storage modulus are in better agreement with DSC T_g, but the T_g was defined as the peak of tan δ due to the peaks' distinctness.

Fig. S10 in SI shows the DSC trace of a M1 homopolymer that was synthesized by free radical polymerization (poly(M1)), and the DSC trace of a crosslinked film of photopolymerized M1. The materials exhibit similar DSC traces with similar T_gs.

The storage modulus tells about the elastic response to the subjected dynamic strain [71]. The obtained storage moduli have been illustrated in Fig. S11. In a crosslinked structure, the storage modulus in the rubbery region relates to the crosslink density of the network [69]. Therefore, the values of storage modulus are plotted in Fig. 6 in dependence of the filler content at 170 °C. That is, in the rubbery plateau region above the glass transition temperature. Fig. 6 shows that the presence of filler slightly increases the storage modulus compared to unfilled matrix. Maximum increases of 56% and 37% are observed for composites with 1% CL and 2% CL, respectively. The clay acts as a physical crosslinker and thus increases the material's degree of crosslinking [69,72]. In other words, this increase can be attributed to increased interactions between the filler and the matrix. These interactions prevent the flow of the matrix chains at high temperatures [73].

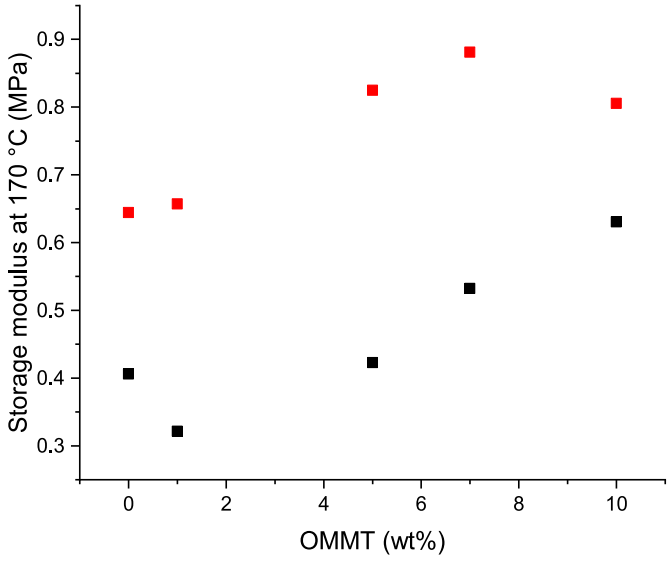

Fig. 6. Storage modulus of composites with 1% (black) and 2% (red) crosslinker at 170 °C in dependence of filler content. (For interpretation of the references to colour in this figure legend, the reader is referred to the Web version of this article.)

3.2. Tensile properties of PIL-OMMT composites

The tensile properties of the composites were determined with stress-strain measurements. Measurements were conducted at room temperature (25 °C) and above the glass transition temperature (T_g), at 140 °C. The purpose was to compare the composites' tensile properties in the glassy and rubbery states. That is because filler additions often offer more prominent improvements in rubbery matrices as opposed to glassy ones [74,75]. The obtained Young's moduli and the failure point stresses and strains have been depicted in Figs. 7 and 9.

In the glassy state, the elastic modulus of a composite with 10 wt% filler almost doubled the Young's modulus compared to the unfilled matrix (Fig. 7A). This indicates positive interaction between the filler and the matrix despite the clay's tendency to aggregate.

Clay also enhanced the mechanical strength of the composites, peaking at certain filler content after which the improvements were less pronounced (Fig. 6B). With 1% crosslinker, the composite was the strongest with 7 wt% filler, exhibiting 1.5 times the strength of unfilled matrix. With 2% crosslinker, maximum strength was obtained with 5 wt % filler content, with which the average strength was 3.6 times as much as that of pristine matrix.

The ductility (Fig. 7C) of the composites does not change significantly as filler is added. The fracture energy of the composites on the other hand increases with the inclusion of filler (Fig. 7D). The toughest materials were obtained with 5 wt% OMMT in the feed.

As was mentioned in the previous section, the fracture surfaces of the stress-strain samples were imaged with scanning electron microscopy (SEM) in order to identify fracture surface morphology. Images of fracture surfaces of composites with 2% CL and various filler loadings are given in Fig. 8. The SEM images from Fig. 8 are also given in Fig. S12 in larger size. The unfilled material exhibited smooth fracture surfaces, which indicates low resistance to crack propagation [12]. Even 1 wt% of clay increases surface roughness in limited areas. Further increase in clay loading increases the surface roughness significantly throughout the fractured surface. The presence of filler causes the cracks to proceed through more tortuous paths. Thus, highly textured fracture surfaces are obtained. The high crack tortuosity accounts for the observed improvements in mechanical properties.

The SEM results support the notion that the filler has a tendency to aggregate. In this case, the decreased strength is attributed to excess filler material aggregating at high filler contents. Since aggregates function as stress concentrators, aggregated materials are weaker than non-aggregated ones [11,73,76].

The composites' tensile properties were characterised also at 140 °C, i.e. above T_g. Above T_g, the properties enhance steadily with increasing

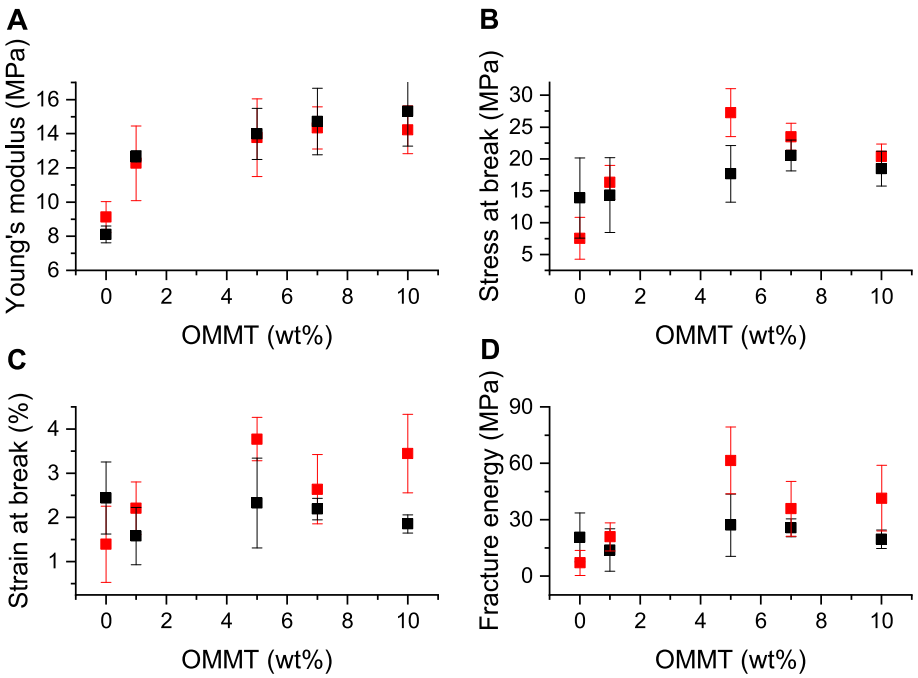

Fig. 7. Tensile properties of composites at 25 °C. A) Young's modulus, B) stress at break, C) strain at break, and D) fracture energy of composites with 1% (black) or 2% (red) crosslinker as a function of organoclay loading. The fracture energy is defined as the area below the stress-strain curve. The values are given as averages of three measurements. (For interpretation of the references to colour in this figure legend, the reader is referred to the Web version of this article.)

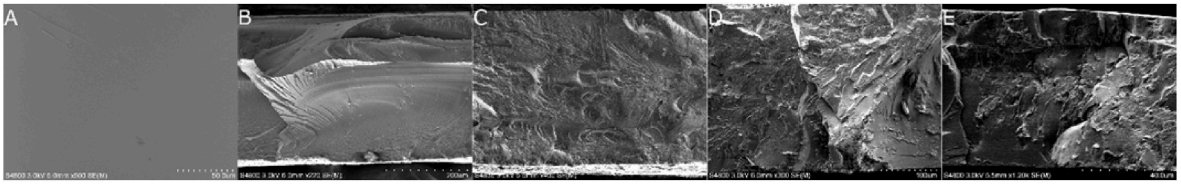

Fig. 8. SEM images of tensile fracture surfaces of composites with 2% crosslinker and A) 0 wt%, B) 1 wt%, C) 5 wt%, D) 7 wt%, and E) 10 wt% OMMT.

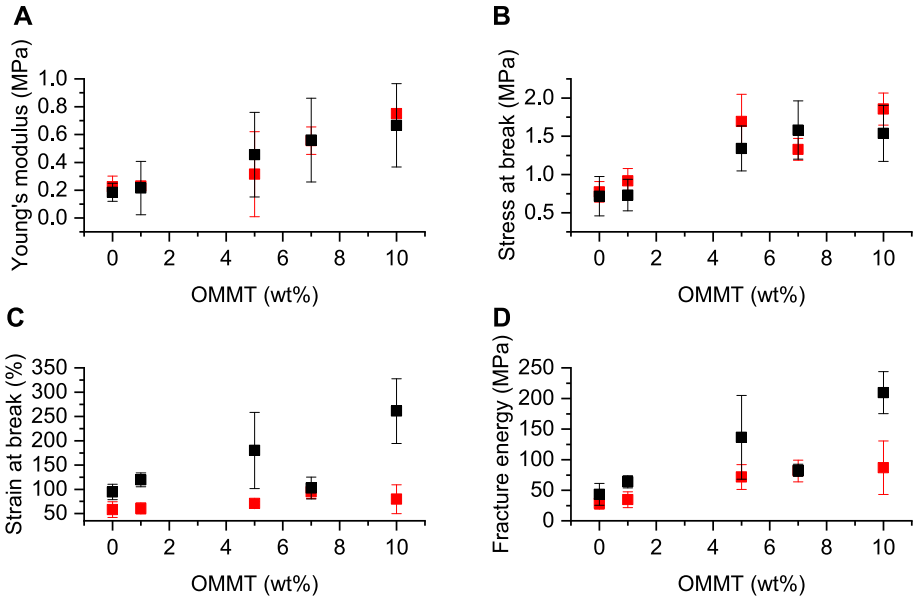

Fig. 9. Tensile properties of composites at 140 °C. A) Young's modulus, B) stress at break, C) strain at break, and D) fracture energy of composites with 1% (black) or 2% (red) crosslinker as a function of filler loading. The values are given as averages of three measurements. (For interpretation of the references to colour in this figure legend, the reader is referred to the Web version of this article.)

filler content (Fig. 9). However, the error margins are wide and hence this inference is to be considered general at best. Unlike at room temperature, at 140 °C the strength of the composites increases up until the highest filler content. The mechanical properties of composites are highly dependent on the nature of the bonds between the filler material and the matrix and the load transfer at the interface [77]. Because interfacial bonding is a prerequisite for stress transfer between the filler and the matrix, the steadily increasing strength indicates that the matrix/filler interactions are strong also at high filler contents.

The most apparent differences between the stress-strain measurements conducted at room temperature and above T_g are seen with the strains at break. Generally filler additions are detrimental to materials' flexibility [72]. Increased crosslink density limits large-scale molecular motions, thus causing embrittlement [72]. However, there are also cases where the maximum elongation increases as filler is added [2,78]. Fig. 9 shows that unlike at room temperature, the strains at break increase with increasing filler content when measured at 140 °C. The strains at break also reveal drastic differences between the composites with different concentrations of covalent crosslinker. The composites with a lower content of covalent crosslinker are far more flexible than the composites with higher concentration of crosslinker.

4. Conclusions

In this contribution, series of PIL-organoclay composites have been prepared with varying clay loadings. The effect of clay on tensile strength, stiffness, elasticity, and thermal phase behaviour of the composites has been studied in dependence of clay content. Increasing clay content led to an increased Young's modulus, both at room temperature and at an elevated temperature. Stress at break reached a peak value at intermediate clay contents, which can be ascribed to arise from excessive aggregation of filler particles at high clay loadings. The aggregation was confirmed by SEM measurements. At room temperature, the clay improved the material strength, while no change was observed in strain at break. High-temperature measurements resulted in enhancements in material stiffness and strength with increasing filler loading.

To summarise, it was observed that the IL monomer dispersed the filler in microscale, and gave glassy composites. The approach of dispersing material in ILs and performing a crosslinking polymerization was shown to be a feasible approach. The methodology will be valuable when designing high-performing composite materials where even filler distribution is key. The improved mechanical properties with increasing filler content indicated successful stress transfer between the matrix and the filler particles. The obtained materials retain their mechanical properties even at high temperatures and are promising as high-temperature engineering rubbers when used above their glass transition temperatures.

CRediT authorship contribution statement

Linda Salminen: Writing – original draft, Data curation, analysis, Investigation, Conceptualization, Methodology, and, Visualization. **Erno Karjalainen:** Supervision, Conceptualization, Methodology, and, Writing – review & editing. **Vladimir Aseyev:** Supervision, and, Writing – review & editing. **Heikki Tenhu:** Project administration, Resources, and, Writing – review & editing.

Declaration of competing interest

The authors declare that they have no known competing financial interests or personal relationships that could have appeared to influence the work reported in this paper.

Data availability

Data will be made available on request.

Acknowledgements

Funding from Emil Aaltonen foundation (210205N) is gratefully acknowledged. SEM imaging and EDX measurements were done in ALD center Finland research infrastructure. Marianna Kemell is gratefully acknowledged for EDX measurements and guidance in SEM imaging.

Appendix B. Supplementary data

Supplementary data to this article can be found online at https://doi.org/10.1016/j.matchemphys.2022.126805.

References

[1] R.K. Shah, D.L. Hunter, D.R. Paul, Nanocomposites from poly(ethylene-co-methacrylic acid) ionomers: effect of surfactant structure on morphology and properties, Polymer 46 (2005) 2646–2662.
[2] Z. Wang, T.J. Pinnavaia, Nanolayer reinforcement of elastomeric polyurethane, Chem. Mater. 10 (1998) 3769–3771, https://doi.org/10.1021/cm980448n.
[3] Y. Kojima, A. Usuki, M. Kawasumi, A. Okada, T. Kurauchi, O. Kamigaito, Synthesis of nylon 6–clay hybrid by montmorillonite intercalated with ε-caprolactam, J. Polym. Sci. Part A Polym Chem 31 (1993) 983–986, https://doi.org/10.1002/pola.1993.080310418.
[4] G. Beyer, Nanocomposites: a new class of flame retardants for polymers, Plastics, Addit. Compd. 4 (2002) 22–28, https://doi.org/10.1016/S1464-391X(02)80151-9.
[5] P. Kiliaris, C.D. Papaspyrides, Polymer/layered silicate (clay) nanocomposites: an overview of flame retardancy, Prog. Polym. Sci. 35 (2010) 902–958.
[6] G. Choudalakis, A.D. Gotsis, Permeability of polymer/clay nanocomposites: a review, Eur. Polym. J. 45 (2009) 967–984, https://doi.org/10.1016/J.EURPOLYMJ.2009.01.027.
[7] P.C. LeBaron, Z. Wang, T.J. Pinnavaia, Polymer-layered silicate nanocomposites: an overview, Appl. Clay Sci. 15 (1999) 11–29, https://doi.org/10.1016/S0169-1317(99)00017-4.
[8] R. Koyilapu, S. Subhadarshini, S. Singha, T. Jana, An in-situ RAFT polymerization technique for the preparation of poly(N-vinyl imidazole) modified Cloisite nanoclay to develop nanocomposite PEM, Polymer 212 (2021), 123175, https://doi.org/10.1016/J.POLYMER.2020.123175.
[9] R. Koyilapu, S. Singha, S.N.R. Kutcherlapati, T. Jana, Grafting of vinylimidazolium-type poly(ionic liquid) on silica nanoparticle through RAFT polymerization for constructing nanocomposite based PEM, Polymer 195 (2020), 122458, https://doi.org/10.1016/J.POLYMER.2020.122458.
[10] B.B. Johnsen, A.J. Kinloch, R.D. Mohammed, A.C. Taylor, S. Sprenger, Toughening mechanisms of nanoparticle-modified epoxy polymers, Polymer 48 (2007) 530–541, https://doi.org/10.1016/J.POLYMER.2006.11.038.
[11] B.T. Marouf, R.A. Pearson, R. Bagheri, Anomalous fracture behavior in an epoxy-based hybrid composite, Mater. Sci. Eng., A 515 (2009) 49–58, https://doi.org/10.1016/j.msea.2009.03.028.
[12] K. Wang, L. Chen, J. Wu, M.L. Toh, C. He, A.F. Yee, Epoxy nanocomposites with highly exfoliated clay : mechanical properties and fracture mechanisms, Macromolecules 38 (2005) 788–800, https://doi.org/10.1021/ma048465n.
[13] S. Xie, S. Zhang, B. Zhao, H. Qin, F. Wang, M. Yang, Tensile fracture morphologies of nylon-6/montmorillonite nanocomposites, Polym. Int. 54 (2005) 1673–1680, https://doi.org/10.1002/PI.1901.
[14] J. Wang, Z. Chen, A. Guan, Qi, N.R. Demarquette, H.E. Naguib, Ionic liquids facilitated dispersion of chitin nanowhiskers for reinforced epoxy composites, Carbohydr. Polym. 247 (2020), 116746, https://doi.org/10.1016/J.CARBPOL.2020.116746.
[15] W. Kitisavetjit, Y. Nakaramontri, S. Pichaiyut, S. Wisunthorn, C. Nakason, S. Kiatkamjornwong, Influences of carbon nanotubes and graphite hybrid filler on properties of natural rubber nanocomposites, Polym. Test. 93 (2021), 106981, https://doi.org/10.1016/J.POLYMERTESTING.2020.106981.
[16] D.F. Santos, A.P.A. Carvalho, B.G. Soares, Phosphonium-based ionic liquid as crosslinker/dispersing agent for epoxy/carbon nanotube nanocomposites: electrical and dynamic mechanical properties, J. Mater. Sci. 55 (2020) 2077–2089, https://doi.org/10.1007/S10853-019-04147-7/TABLES/2.
[17] R.P. Swatloski, S.K. Spear, J.D. Holbrey, R.D. Rogers, Dissolution of cellose with ionic liquids, J. Am. Chem. Soc. 124 (2002) 4974–4975, https://doi.org/10.1021/ja025790m.
[18] M.L. Polo-Luque, B.M. Simonet, M. Valcárcel, Functionalization and dispersion of carbon nanotubes in ionic liquids, TrAC, Trends Anal. Chem. 47 (2013) 99–110, https://doi.org/10.1016/j.trac.2013.03.007.
[19] R. Peng, Y. Wang, W. Tang, Y. Yang, X. Xie, Progress in imidazolium ionic liquids assisted fabrication of carbon nanotube and graphene polymer composites, Polymers 5 (2013) 847–872, https://doi.org/10.3390/polym5020847.
[20] S. Wellens, T. Vander Hoogerstraete, C. Möller, B. Thijs, J. Luyten, K. Binnemans, Dissolution of metal oxides in an acid-saturated ionic liquid solution and investigation of the back-extraction behaviour to the aqueous phase, Hydrometallurgy 144–145 (2014) 27–33, https://doi.org/10.1016/j.hydromet.2014.01.015.
[21] A.P. Abbott, G. Frisch, J. Hartley, W.O. Karim, K.S. Ryder, Anodic dissolution of metals in ionic liquids, Prog. Nat. Sci. Mater. Int. 25 (2015) 595–602, https://doi.org/10.1016/j.pnsc.2015.11.005.

[22] A. Xu, J. Wang, H. Wang, Effects of anionic structure and lithium salts addition on the dissolution of cellulose in 1-butyl-3-methylimidazolium-based ionic liquid solvent systems, Green Chem. 12 (2010) 268, https://doi.org/10.1039/b916882f, 27.
[23] J. Yuan, D. Mecerreyes, M. Antonietti, Poly(ionic liquid)s: an update, Prog. Polym. Sci. 38 (2013) 1009–1036, https://doi.org/10.1016/j.progpolymsci.2013.04.002.
[24] W. Qian, J. Texter, F. Yan, Frontiers in poly(ionic liquid)s: syntheses and applications, Chem. Soc. Rev. 46 (2017) 1124–1159, https://doi.org/10.1039/c6cs00620e.
[25] P. Bonhôte, A.P. Dias, N. Papageorgiou, K. Kalyanasundaram, M. Grätzel, Hydrophobic, highly conductive ambient-temperature molten salts, Inorg. Chem. 35 (1996) 1168–1178, https://doi.org/10.1021/ic951325x.
[26] N. Papaiconomou, N. Yakelis, J. Salminen, R. Bergman, J.M. Prausnitz, Synthesis and properties of seven ionic liquids containing 1-Methyl-3-octylimidazolium or 1-Butyl-4-methylpyridinium cations, J. Chem. Eng. Data 51 (2006) 1389–1393, https://doi.org/10.1021/JE060096Y.
[27] M.G. Freire, L.M.N.B.F. Santos, A.M. Fernandes, J.A.P. Coutinho, I.M. Marrucho, An overview of the mutual solubilities of water–imidazolium-based ionic liquids systems, Fluid Phase Equil. 261 (2007) 449–454.
[28] J. Texter, Anion responsive imidazolium-based polymers, Macromol. Rapid Commun. 33 (2012) 1996, https://doi.org/10.1002/marc.201200525. –2014.
[29] M.D. Green, D. Salas-De La Cruz, Y. Ye, J.M. Layman, Y.A. Elabd, K.I. Winey, et al., Alkyl-substituted N-vinylimidazolium polymerized ionic liquids: thermal properties and ionic conductivities, Macromol. Chem. Phys. 212 (2011) 2522–2528, https://doi.org/10.1002/macp.201100389.
[30] Y. Ye, Y.A. Elabd, Anion exchanged polymerized ionic liquids: high free volume single ion conductors, Polymer 52 (2011) 1309–1317, https://doi.org/10.1016/j.polymer.2011.01.031.
[31] K. Nakamura, K. Fukao, T. Inoue, Dielectric relaxation and viscoelastic behavior of polymerized ionic liquids with various counteranions, Macromolecules 45 (2012) 3850–3858, https://doi.org/10.1021/ma300040b.
[32] R. Marcilla, J.A. Blazquez, J. Rodriguez, J.A. Pomposo, D. Mecerreyes, Tuning the solubility of polymerized ionic liquids by simple anion-exchange reactions, J. Polym. Sci. Part A Polym Chem 42 (2004) 208–212, https://doi.org/10.1002/pola.11015.
[33] R. Marcilla, J.A. Blazquez, R. Fernandez, H. Grande, J.A. Pomposo, D. Mecerreyes, Synthesis of novel polycations using the chemistry of ionic liquids, Macromol. Chem. Phys. 206 (2005) 299–304, https://doi.org/10.1002/macp.200400411.
[34] A.S. Shaplov, E.I. Lozinskaya, D.O. Ponkratov, I.A. Malyshkina, F. Vidal, P.-H. Aubert, et al., Bis(trifluoromethylsulfonyl)amide based “polymeric ionic liquids”: synthesis, purification and pecularities of structure-properties relationships, Electrochim. Acta 57 (2011) 74–90.
[35] R.S. Bhavsar, S.C. Kumbharkar, A.S. Rewar, U.K. Kharul, Polybenzimidazole based film forming polymeric ionic liquids: synthesis and effects of cation-anion variation on their physical properties, Polym. Chem. 5 (2014) 4083–4096, https://doi.org/10.1039/c3py01709e.
[36] A.L. Pont, R. Marcilla, I. De Meatza, H. Grande, D. Mecerreyes, Pyrrolidinium-based polymeric ionic liquids as mechanically and electrochemically stable polymer electrolytes, J. Power Sources 188 (2009) 558–563, https://doi.org/10.1016/j.jpowsour.2008.11.115.
[37] A.S. Shaplov, D.O. Ponkratov, P.S. Vlasov, E.I. Lozinskaya, L.V. Gumileva, C. Surcin, et al., Ionic semi-interpenetrating networks as a new approach for highly conductive and stretchable polymer materials, J. Mater. Chem. 3 (2015) 2188–2198, https://doi.org/10.1039/c4ta05833j.
[38] G.B. Appetecchi, G.-T. Kim, M. Montanino, M. Carewska, R. Marcilla, D. Mecerreyes, et al., Ternary polymer electrolytes containing pyrrolidinium-based polymeric ionic liquids for lithium batteries, J. Power Sources 195 (2010) 3668–3675, https://doi.org/10.1016/j.jpowsour.2009.11.146.
[39] E. Karjalainen, D.J. Wales, D.H.A.T. Gunasekera, J. Dupont, P. Licence, R. D. Wildman, et al., Tunable ionic control of polymeric films for inkjet based 3D printing, ACS Sustain. Chem. Eng. 6 (2018) 3984–3991, https://doi.org/10.1021/acssuschemeng.7b04279.
[40] D.J. Wales, Q. Cao, K. Kastner, E. Karjalainen, G.N. Newton, V. Sans, 3D-Printable photochromic molecular materials for reversible information storage, Adv. Mater. 30 (2018) 1–7, https://doi.org/10.1002/adma.201800159.
[41] T. Fukushima, A. Kosaka, Y. Yamamoto, T. Aimiya, S. Notazawa, T. Takigawa, et al., Dramatic effect of dispersed carbon nanotubes on the mechanical and electroconductive properties of polymers derived from ionic liquids, Small 2 (2006) 554–560, https://doi.org/10.1002/smll.200500404.
[42] T. Fukushima, A. Kosaka, Y. Ishimura, T. Yamamoto, T. Takigawa, N. Ishii, et al., Molecular ordering of organic molten salts triggered by single-walled carbon nanotubes, Science 300 (80) (2003) 2072, https://doi.org/10.1126/science.1082289, 4.
[43] T. Fukushima, T. Aida, Ionic liquids for soft functional materials with carbon nanotubes, Chem. Eur J. 13 (2007) 5048–5058, https://doi.org/10.1002/chem.200700554.
[44] J. Lee, T. Aida, Bucky gels” for tailoring electroactive materials and devices: the composites of carbon materials with ionic liquids, Chem. Commun. 47 (2011) 6757–6762, https://doi.org/10.1039/c1cc00043h.
[45] J.A. Throckmorton, A.L. Watters, X. Geng, G.R. Palmese, Room temperature ionic liquids for epoxy nanocomposite synthesis: direct dispersion and cure, Compos. Sci. Technol. 86 (2013) 38–44.
[46] K. Prasad, J. Kadokawa, Preparation of composite materials composed of ι-carrageenan and polymeric ionic liquids, Polym. Compos. 31 (2010) 799–806, https://doi.org/10.1002/pc.20862.
[47] M aki Murakami, Y. Kaneko, J ichi Kadokawa, Preparation of cellulose-polymerized ionic liquid composite by in-situ polymerization of polymerizable ionic liquid in cellulose-dissolving solution, Carbohydr. Polym. 69 (2007) 378–381, https://doi.org/10.1016/j.carbpol.2006.12.002.
[48] J ichi Kadokawa, M aki Murakami, Y. Kaneko, A facile method for preparation of composites composed of cellulose and a polystyrene-type polymeric ionic liquid using a polymerizable ionic liquid, Compos. Sci. Technol. 68 (2008) 493–498, https://doi.org/10.1016/j.compscitech.2007.06.004.
[49] A. Takegawa, M. Murakami, Y. Kaneko, J. Kadokawa, A facile preparation of composites composed of cellulose and polymeric ionic liquids by in situ polymerization of ionic liquids having acrylate groups, Polym. Compos. 30 (2009) 1837–1841, https://doi.org/10.1002/pc.20756.
[50] M. Setoyama, T. Kato, K. Yamamoto, J.-I. Kadokawa, Preparation of chitin/cellulose films compatibilized with polymeric ionic liquids, J. Polym. Environ. 21 (2013) 795–801, https://doi.org/10.1007/s10924-013-0580-4.
[51] T. Mizumo, T. Watanabe, N. Matsumi, H. Ohno, Preparation of ion conductive inorganic–organic composite systems by in situ sol–gel reaction of polymerizable ionic liquids, Polym. Adv. Technol. 19 (2008) 1445–1450, https://doi.org/10.1002/pat.1221.
[52] R. Löwe, T. Hanemann, T. Zinkevich, A. Hofmann, Poly(ionic liquid) based composite electrolytes for lithium ion batteries, Polymers 13 (2021) 4469, https://doi.org/10.3390/polym13244469.
[53] A. Leszczyńska, J. Njuguna, K. Pielichowski, J.R. Banerjee, Polymer/montmorillonite nanocomposites with improved thermal properties: Part II. Thermal stability of montmorillonite nanocomposites based on different polymeric matrixes, Thermochim. Acta 454 (2007) 1–22, https://doi.org/10.1016/J.TCA.2006.11.003.
[54] S. Sinha Ray, M. Okamoto, Polymer/layered silica nanocomposites: a review from preparation to processing, Prog. Polym. Sci. 28 (2003) 1539–1641.
[55] Q.T. Nguyen, D.G. Baird, Preparation of polymer–clay nanocomposites and their properties, Adv. Polym. Technol. 25 (2006) 270–285, https://doi.org/10.1002/adv.
[56] H. He, Z. Ding, J. Zhu, P. Yuan, Y. Xi, D. Yang, et al., Thermal characterization of surfactant-modified montmorillonites, Clay Clay Miner. 53 (2005) 287–293, https://doi.org/10.1346/CCMN.2005.0530308.
[57] Z. Wen, W. Jincheng, Preparation and characterization of a cyclophosphamide-core PAMAM dendritic montmorillonite, Silicon 10 (2018) 483–493, https://doi.org/10.1007/s12633-016-9478-9.
[58] C.-W. Chiu, T.-K. Huang, Y.-C. Wang, B. Alamani, J.-J. Lin, Intercalation strategies in clay/polymer hybrids, Prog. Polym. Sci. 39 (2014) 443–485.
[59] R.A. Vaia, R.K. Teukolsky, E.P. Giannelis, Interlayer structure and molecular environment of alkylammonium layered silicates, Chem. Mater. 6 (1994) 1017–1022, https://doi.org/10.1021/cm00043a025.
[60] Y. Shen, Y. Wang, J. Chen, H. Li, Z. Li, C. Li, Nitroxide-mediated polymerization of styrene initiated from the surface of montmorillonite clay platelets, J. Appl. Polym. Sci. 118 (2010) 1198–1203, https://doi.org/10.1002/APP.32498.
[61] T.T. Zhu, C.H. Zhou, F.B. Kabwe, Q.Q. Wu, C.S. Li, J.R. Zhang, Exfoliation of montmorillonite and related properties of clay/polymer nanocomposites, Appl. Clay Sci. 169 (2019) 48–66, https://doi.org/10.1016/J.CLAY.2018.12.006.
[62] F.F. Lange, The interaction of a crack front with a second-phase dispersion, Philos. Mag. A 22 (1970) 983–992, https://doi.org/10.1080/14786437008221068.
[63] K. Nakamura, T. Saiwaki, K. Fukao, T. Inoue, Viscoelastic behavior of the polymerized ionic liquid poly(1-ethyl-3- vinylimidazolium bis (trifluoromethanesulfonylimide)), Macromolecules 44 (2011) 7719–7726, https://doi.org/10.1021/ma201611q.
[64] K. Nakamura, K. Fukao, Dielectric relaxation behavior of polymerized ionic liquids with various charge densities, Polymer 54 (2013) 3306–3313, https://doi.org/10.1016/J.POLYMER.2013.04.039.
[65] K. Nakamura, T. Saiwaki, K. Fukao, Dielectric relaxation behavior of polymerized ionic liquid, Macromolecules 43 (2010) 6092–6098, https://doi.org/10.1021/MA100918E/SUPPL_FILE/MA100918E_SI_001.PDF.
[66] B.L. Lee, L.E. Nielsen, Temperature dependence of the dynamic mechanical properties of filled polymers, J. Polym. Sci. Polym. Phys. Ed 15 (1977) 683–692, https://doi.org/10.1002/pol.1977.180150408.
[67] A. Bansal, H. Yang, C. Li, B.C. Benicewicz, S.K. Kumar, L.S. Schadler, Controlling the thermomechanical properties of polymer nanocomposites by tailoring the polymer–particle interface, J. Polym. Sci., Part B: Polym. Phys. 44 (2006) 2944–2950, https://doi.org/10.1002/polb.
[68] M.M. Rahman, H.-D. Kim, W.-K. Lee, Preparation and characterization of waterborne polyurethane/clay nanocomposite: effect on water vapor permeability, J. Appl. Polym. Sci. 110 (2008) 3697–3705, https://doi.org/10.1002/app.28985.
[69] S. Zhang, A. Yu, S. Liu, J. Zhao, J. Jiang, X. Liu, Effect of silica nanoparticles on structure and properties of waterborne UV-curable polyurethane nanocomposites, Polym. Bull. 68 (2012) 1469–1482, https://doi.org/10.1007/s00289-011-0689-3.
[70] A. Bansal, H. Yang, C. Li, K. Cho, B.C. Benicewicz, S.K. Kumar, et al., Quantitative equivalence between polymer nanocomposites and thin polymer films, Nat. Mater. 4 (2005) 693–698, https://doi.org/10.1038/nmat1447.
[71] C. Becker, H. Krug, H. Schmidt, Tailoring of thermomechanical properties of thermoplastic nanocomposites by surface modification of nanoscale silica particles, MRS Proc. 435 (1996) 237.
[72] K.T. Gam, M. Miyamoto, R. Nishimura, H.-J. Sue, Fracture behavior of core-shell rubber-modified clay-epoxy nanocomposites, Polym. Eng. Sci. 43 (2003) 1635–1645.
[73] A. Dufresne, M. Paillet, J.L. Putaux, A.A. Schweitzer, Processing and characterization of carbon nanotube/poly (styrene-co-butyl acrylate) nanocomposites, J. Mater. Sci. 37 (2002) 3915–3923.

[74] D. Ratna, N.R. Manoj, R. Varley, R.K. Singh Raman, G.P. Simon, Clay-reinforced epoxy nanocomposites, Polym. Int. 52 (2003) 1403–1407, https://doi.org/10.1002/PI.1166.
[75] T. Lan, T.J. Pinnavaia, Clay-Reinforced epoxy, Chem. Mater. 6 (1994) 2216–2219.
[76] I.Y. Phang, T. Liu, A. Mohamed, K.P. Pramoda, L. Chen, L. Shen, et al., Morphology, thermal and mechanical properties of nylon 12/organoclay nanocomposites prepared by melt compounding, Polym. Int. 54 (2005) 456–464, https://doi.org/10.1002/pi.1721.
[77] N. Alberola, A. Bergeret, Physical modeling of the interphase in amorphous thermoplastic/glass bead composites, Polym. Compos. 15 (1994) 442–452, https://doi.org/10.1002/pc.750150609.
[78] J. Ma, Z. Qi, S. Zhang, Synthesis and characterization of elastomeric polyurethane/clay nanocomposites, J. Appl. Polym. Sci. 82 (2001) 1444–1448.